Dual Series Solution to the Scattering of Plane Waves from a Binary Conducting Grating

YON-LIN KOK, ASSOCIATE MEMBER, IEEE, NEAL C. GALLAGHER, JR., FELLOW, IEEE, AND RICHARD W. ZIOLKOWSKI, MEMBER, IEEE

Abstract—**The problem of scattering by electromagnetic waves from a perfectly conducting grating with periodic groove structure is considered. A system of dual series equations has been derived by enforcing the electromagnetic boundary conditions; this leads to a boundary value problem that is successfully solved. The mathematics leading to the solution of the dual series system is derived from the equivalent Riemann-Hilbert problem in complex variable theory and its solution. The solution converges absolutely and allows one to obtain analytical results, even where other numerical methods, such as the mode-matching method and the spectral iteration method, are numerically unstable. As most papers consider only diffraction efficiencies in the grating problems, we are also interested in the relative phase values for the diffracted fields. The phase differences between the scattered fields resulting from two orthogonally polarized incident plane waves can be explicitly determined for any incidence angles and for any groove dimensions. Comparisons with the results from the mode-matching method and the spectral-iteration method are also given.**

I. INTRODUCTION

DURING THE LAST TWO decades several approaches have been taken in studying the properties of light diffracted by perfectly conducting diffraction gratings. Methods such as the spectral-iteration method [1] and the mode-matching method [2] have been used to study the diffraction efficiencies of those gratings. A thorough review of some of these diffraction theories can be found in [2]–[4]. As most papers consider only diffraction efficiency calculations, we are also interested in the phase value calculations for the diffracted fields. We find that the phase value calculations are much more sensitive to numerical error than diffraction efficiency calculations. Even so, can one trust a diffraction efficiency calculation, when the phase calculation has large error?

In a previous paper [5], Kok and Gallagher employ the mode-matching method in solving the phase variation associated with an arbitrarily incident electromagnetic wave diffracted by a perfectly conducting, groove-corrugated surface (Fig. 1). Starting with the electromagnetic wave equation, they represented the field in terms of a Floquet–Bloch expansion in the half-open region while the field inside the groove region is expanded in a Fourier series. They found that purely numerical methods (e.g., spectral-iteration method and mode-matching method) may encounter difficulties mainly due to the discontinuous behavior of the associated field function at the electromagnetic boundary.

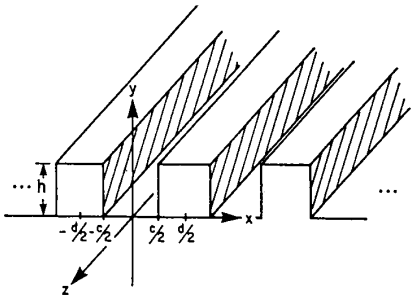

Fig. 1. The perfectly conducting groove surface in a rectangular coordinate system. The groove structure is periodic in the x-axis direction with groove period d, groove width c and groove depth h. The grooves are infinitely long and uniform in the z-axis direction.

Recent developments in the theories and applications of dual series equations [6] and their relationship to the Riemann–Hilbert problem [7] have made it possible to obtain analytical solutions to families of canonical problems descriptive of electromagnetic coupling via apertures into enclosed and open regions [8], [9]. These coupling problems constitute only a small subset of a large class of mixed boundary value problems. Plane wave diffraction by a perfectly conducting grating of infinitesimal thickness is one of the canonical problems amenable to solutions from these techniques [10]. Once the boundary value problem is solved, one can easily assure convergence and compute the modal coefficients and the subsequent wave functions.

In this paper we will exploit the general dual series equations and Riemann–Hilbert techniques in analyzing the problem of plane wave diffraction by a perfectly conducting, groove-corrugated surface. Wave solutions subject to the boundary conditions imposed by the groove structures are given in Section II. There we define a general electromagnetic wave in terms of two orthogonal components: *fast polarization* and *slow polarization*; and the diffraction problem is then treated for each of these cases independently. A system of dual series equations is derived for each case. The connections between the general dual series equations and the Riemann–Hilbert problems will be given in Section III. Rigorous solutions of the modal coefficients and the phase variations in both the fast and the slow polarization cases are obtained by solving a system of linear equations. In Section IV we discuss

Manuscript received July 16, 1987; revised February 9, 1988.

Y. L. Kok was with the School of Electrical Engineering, Purdue University, West Lafayette, IN. He is now with the Department of Electrical Engineering, University of South Alabama, Mobile, AL 36688.

N. C. Gallagher, Jr. is with the School of Electrical Engineering, Purdue University, West Lafayette, IN 47907.

R. W. Ziolkowski is with the Engineering Research Division, Lawrence Livermore National Laboratory, Livermore, CA 94550.

IEEE Log Number 8927662.

0018-926X/89/0700-0901$01.00

various aspects of the phase angle difference between these two orthogonally polarized waves. The convergence in computing the phase differences with dual series method is also illustrated there. In particular, the solution to the Riemann–Hilbert problem is generalized to the case where the forcing function ($F_0(z)$ in (24), Section III-A) is multivalued in the complex variable z-plane.

Brief comparisons between the results from the iteration method, the mode-matching method, and the Riemann–Hilbert approach are also given. They demonstrate that the Riemann–Hilbert approach works the best for all groove dimensions and all spectral regions.

II. Analysis

A. Field Solutions

Assume that a monochromatic plane wave is incident on the perfectly conducting, groove-corrugated planar surface (x-z plane in a rectangular coordinate system) shown in Fig. 1. The grooves of rectangular shape are infinitely long in the z-axis direction. They exist periodically in the x-axis direction with period d. Groove width and groove depth are defined to be c and h, respectively. The associated wave vector of the incident plane wave $\vec{k}$ can be represented by $\hat{x}\alpha_0 - \hat{y}\beta_0 + \hat{z}\gamma$, so that the incident electric field has a phase variation of the form, $\exp[i(\alpha_0 x - \beta_0 y + \gamma z)]$, where $\alpha_0 = k\cos\theta\cos\phi$, $\beta_0 = k\sin\theta\cos\phi$, $\gamma = k\sin\phi$ and $k = \omega(\mu\epsilon)^{1/2}$. This is illustrated in Fig. 2. The incident electric field is assumed to have unit amplitude. We decompose the electromagnetic wave into two orthogonal components [5]: the *fast polarization* component and the *slow polarization* component, in each of the following two regions.

1) Region 1 ($y \geq h$)

(a) Fast polarization

$$E = \left[\frac{i\sin\phi}{k}\frac{\partial U}{\partial x}, \frac{i\sin\phi}{k}\frac{\partial U}{\partial y}, U\cos^2\phi\right] \tag{1}$$

$$H = \left[\frac{-i}{\omega\mu}\frac{\partial U}{\partial y}, \frac{i}{\omega\mu}\frac{\partial U}{\partial x}, 0\right] \tag{2}$$

where

$$U(x, y, z) = \exp[i(\alpha_0 x - \beta_0 y + \gamma z)] + \sum_{n=-\infty}^{\infty} r_n \exp[i(\alpha_n x + \beta_n y + \gamma z)]$$

$$\alpha_n = \alpha_0 + \frac{2\pi}{d}n, \quad \beta_n = (k^2 - \alpha_n^2 - \gamma^2)^{1/2}.$$

(b) Slow polarization

$$H = \left[\frac{i\sin\phi}{k}\frac{\partial V}{\partial x}, \frac{i\sin\phi}{k}\frac{\partial V}{\partial y}, V\cos^2\phi\right] \tag{3}$$

$$E = \left[\frac{i}{\omega\epsilon}\frac{\partial V}{\partial y}, \frac{-i}{\omega\epsilon}\frac{\partial V}{\partial x}, 0\right] \tag{4}$$

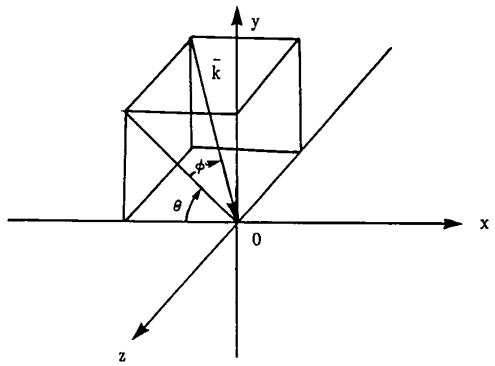

Fig. 2. Definitions of the incident wave angles: ϕ and θ. $\vec{k}$ is the wave vector of the incident plane wave. ϕ is the angle between $\vec{k}$ and its projection on the x-y plane. θ is the angle between the projection of $\vec{k}$ on the x-y plane and the x-axis.

where

$$V(x, y, z) = \exp[i(\alpha_0 x - \beta_0 y + \gamma z)] + \sum_{n=-\infty}^{\infty} s_n \exp[i(\alpha_n x + \beta_n y + \gamma z)].$$

2) Region 2 ($0 \leq y < h$)

(a) Fast polarization

$$E_z(x, y, z) = \begin{cases} \sum_{n=1}^{\infty} a_n \sin\left[\frac{n\pi}{c}\left(x + \frac{c}{2}\right)\right] \sin(A_n y) \\ \quad \cdot \exp(i\gamma z), & 0 \leq |x| < \frac{c}{2}, \\ 0, & \frac{c}{2} < |x| \leq \frac{d}{2}. \end{cases} \tag{5}$$

where

$$A_n^2 = k^2 - \left(\frac{n\pi}{c}\right)^2 - \gamma^2, \qquad n = 1, 2, 3, \cdots.$$

The term $\sin(A_n y)$ is replaced by $\sinh(\bar{A}_n y)$ if

$$k^2 - \left(\frac{\pi n}{c}\right)^2 - \gamma^2 < 0, \quad \text{so that } \bar{A}_n = \sqrt{\gamma^2 + \left(\frac{\pi n}{c}\right)^2 - k^2}.$$

Other field components can be obtained directly from Maxwell's equation;

$$E_x = \frac{i\gamma}{\hbar^2}\frac{\partial E_z}{\partial x}, \quad E_y = \frac{i\gamma}{\hbar^2}\frac{\partial E_z}{\partial y}, \quad H_x = \frac{-i\omega\epsilon}{\hbar^2}\frac{\partial E_z}{\partial y}, \quad H_y = \frac{i\omega\epsilon}{\hbar^2}\frac{\partial E_z}{\partial x}$$

where $\hbar = k\cos\phi$.

(b) Slow Polarization

$$H_z = \sum_{n=0}^{\infty} b_n \cos\left[\frac{n\pi}{c}\left(x + \frac{c}{2}\right)\right] \cos(B_n y) \exp(i\gamma z), \qquad 0 \leq |x| < \frac{c}{2} \tag{6}$$

where

$$B_n^2 = k^2 - \left(\frac{n\pi}{c}\right)^2 - \gamma^2, \qquad n = 0, 1, 2, \cdots.$$

The term $\cos(B_n y)$ is replaced by $\cosh(\bar{B}_n y)$ if

$$k^2 - \left(\frac{\pi n}{c}\right)^2 - \gamma^2 < 0, \quad \text{so that } \bar{B}_n = \sqrt{\gamma^2 + \left(\frac{\pi n}{c}\right)^2 - k^2}.$$

Similar to the fast polarization case, we can derive other field components from Maxwell's equations;

$$E_x = \frac{i\omega\mu}{\hbar^2}\frac{\partial H_z}{\partial y}, \quad E_y = -\frac{i\omega\mu}{\hbar^2}\frac{\partial H_z}{\partial x},$$

$$H_x = \frac{i\gamma}{\hbar^2}\frac{\partial H_z}{\partial x}, \quad H_y = \frac{i\gamma}{\hbar^2}\frac{\partial H_z}{\partial y}.$$

B. Matching the Tangential Fields at $y = h$

Consider the tangential fields in one period of the groove structure (i.e., $0 \le |x| \le d/2$). At the interface between regions 1 and 2, $y = h$, the electromagnetic boundary conditions require that the tangential E-field be continuous for all x while the tangential H-field be continuous within the aperture of the groove (i.e., $0 \le |x| < c/2$). For each of the two orthogonal polarization components one then obtains the following results.

1) Fast polarization

(a) $E_z(x, y, z)|_{y=h}$ is continuous for $0 \le |x| < d/2$: Referring to (1) and (5) for the field function $E_z(x, y, z)|_{y=h}$, we have

$$\cos^2\phi \left\{\exp\left[i(\alpha_0 x - \beta_0 h + \gamma z)\right] + \sum_{n=-\infty}^{\infty} r_n \exp\left[i(\alpha_n x + \beta_n h + \gamma z)\right]\right\}$$

$$= \begin{cases} \displaystyle\sum_{n=1}^{\infty} a_n \sin\left[\frac{n\pi}{c}\left(x + \frac{c}{2}\right)\right] \sin(A_n h) \\ \quad \cdot \exp(i\gamma z), \qquad 0 \le |x| < \dfrac{c}{2} \\ 0, \qquad \dfrac{c}{2} < |x| \le \dfrac{d}{2}. \end{cases} \tag{7}$$

(b) $H_x(x, y, z)|_{y=h}$ is continuous for $0 \le |x| < c/2$: From (2) and the partial derivative of (5) with respect to y, we have the wave function $H_x(x, y, z)|_{y=h}$. Imposing the condition of continuity then yields;

$$\left(\frac{-i}{\omega\mu}\right)\left\{(-i\beta_0)\exp\left[i(\alpha_0 x - \beta_0 h + \gamma z)\right] + \sum_{n=-\infty}^{\infty} r_n (i\beta_n)\exp\left[i(\alpha_n x + \beta_n h + \gamma z)\right]\right\}$$

$$= \left(\frac{-i\omega\epsilon}{\hbar^2}\right)\sum_{n=1}^{\infty} a_n A_n \sin\left[\frac{n\pi}{c}\left(x + \frac{c}{2}\right)\right] \cdot \cos(A_n h)\exp(i\gamma z), \qquad 0 \le |x| < \frac{c}{2}. \tag{8}$$

2) Slow Polarization:

(a) $H_z(x, y, z)|_{y=h}$ is continuous for $0 \le |x| < c/2$: Referring to (3) and (6) for the wave function $H_z(x, y, z)|_{y=h}$, we have

$$\cos^2\phi \left\{\exp\left[i(\alpha_0 x - \beta_0 h + \gamma z)\right] + \sum_{n=-\infty}^{\infty} s_n \exp\left[i(\alpha_n x + \beta_n y + \gamma z)\right]\right\}$$

$$= \sum_{n=0}^{\infty} b_n \cos(B_n h) \cos\left[\frac{n\pi}{c}\left(x + \frac{c}{2}\right)\right] \cdot \exp(i\gamma z), \qquad 0 \le |x| < \frac{c}{2}. \tag{9}$$

(b) $E_x(x, y, z)|_{y=h}$ is continuous for $0 \le |x| \le d/2$: Referring to (4) and the partial derivative of (6) with respect to y for the representations of E_x, we impose the condition of continuity:

$$\left(\frac{i}{\omega\epsilon}\right)\left\{(-i\beta_0)\exp\left[i(\alpha_0 x - \beta_0 h + \gamma z)\right] + \sum_{n=-\infty}^{\infty} s_n (i\beta_n)\exp\left[i(\alpha_n x + \beta_n h + \gamma z)\right]\right\}$$

$$= \begin{cases} \left(\dfrac{i\omega\mu}{\hbar^2}\right)\displaystyle\sum_{n=0}^{\infty}(-b_n B_n)\cos\left[\frac{n\pi}{c}\left(x + \frac{c}{2}\right)\right] \\ \quad \cdot \sin(B_n h)\exp(i\gamma z), \qquad 0 \le |x| < \dfrac{c}{2} \\ 0, \qquad \dfrac{c}{2} < |x| \le \dfrac{d}{2} \end{cases} \tag{10}$$

Now we have two pairs of unknowns, r_n, a_n and s_n, b_n in (7)–(10). In the following sections we formulate these equations into a dual series form for both the fast and the slow polarization cases. Then we apply the techniques borrowed from Riemann-Hilbert problems [11] in solving for the unknowns.

C. Dual Series Representation

1) Fast Polarization Case: Rewrite (7) and (8) in the following form. For $0 \le |x| < c/2$,

$$(\cos^2\phi)\left\{\exp(-i\beta_0 h) + \sum_{n=-\infty}^{\infty} r_n \cdot \exp\left[i\left(\frac{2\pi}{d}nx + \beta_n h\right)\right]\right\} = \sum_{n=1}^{\infty} a_n \sin(A_n h)\sin\left[\frac{n\pi}{c}\left(x + \frac{c}{2}\right)\right] \cdot \exp(-i\alpha_0 x), \tag{11}$$

$$(\cos^2\phi)\left\{(-i\beta_0)\exp(-i\beta_0 h)+\sum_{n=-\infty}^{\infty}(i\beta_n r_n)\cdot\exp\left[i\left(\frac{2\pi}{d}nx+\beta_n h\right)\right]\right\}$$
$$=\sum_{n=1}^{\infty}a_n A_n\cos(A_n h)\sin\left[\frac{n\pi}{c}\left(x+\frac{c}{2}\right)\right]\cdot\exp(-i\alpha_0 x). \quad (12)$$

For $c/2 < |x| \le d/2$,

$$(\cos^2\phi)\left\{\exp(-i\beta_0 h)+\sum_{n=-\infty}^{\infty}r_n\cdot\exp\left[i\left(\frac{2\pi}{d}nx+\beta_n h\right)\right]\right\}=0. \quad (13)$$

A system of dual series is derived from (11), (12), and (13) (Appendix I);

$$\sum_{m=-\infty}^{\infty}\eta_m\exp(im\psi)=0,\qquad \text{for } \psi_0<|\psi|\le\pi \quad (14)$$

$$\sum_{m=-\infty}^{\infty}\eta_m|m|\exp(im\psi)=\xi\eta_0+\sum_{m=-\infty}^{\infty}f_m\exp(im\psi)+\sum_{n=-\infty}^{\infty}g_n\exp[i(n\nu-\tau)\psi,\qquad \text{for } 0\le|\psi|<\psi_0 \quad (15)$$

where

$$\eta_0=\exp(-i\beta_0 h)+r_0\exp(i\beta_0 h)$$
$$\eta_n=r_n\exp(i\beta_n h),\qquad n\ne 0$$
$$\xi=id\beta_0/2\pi,$$
$$f_m=\begin{cases}-id\beta_0\exp(-i\beta_0 h)/\pi, & m=0\\ \eta_m|m|\epsilon_m, & m\ne 0\end{cases}$$
$$g_n=\begin{cases}0, & n=0\\ \left(\dfrac{-d}{4\pi}\right)A_n\cot(A_n h)\displaystyle\sum_{m=-\infty}^{\infty}\eta_m\cdot t_{nm}\cdot u_{nm}, & n\ne 0\end{cases}$$
$$t_{nm}=\begin{cases}(-1)^n\exp[-i(\alpha_m c+n\pi)/2], & n>0\\ \exp[-i(\alpha_m c+n\pi)/2], & n<0\end{cases}$$
$$u_{nm}=\begin{cases}\pm 1, & \alpha_m c=\pm n\pi\\ \dfrac{(-i2\pi n)[(-1)^n\exp(i\alpha_m c)-1]}{(\alpha_m c)^2-(n\pi)^2}, & \alpha_m c\ne\pm n\pi\end{cases}$$
$$\nu=d/(2c),$$
$$\tau=\alpha_0 d/2\pi,$$
$$\psi_0=c\pi/d,$$
$$\epsilon_m=1-\sqrt{[(\alpha_0 d/2\pi m)+1]^2-(dh/2\pi m)^2}.$$

Equations (14) and (15) constitute a dual series system with unknown coefficients η_m, $m = 0, \pm 1, \pm 2, \cdots$, for the fast polarization wave.

2) Slow Polarization: Rewrite (9) and (10) in the following form. For $0 \le |x| < c/2$,

$$\cos^2\phi\left\{\exp(-i\beta_0 h)+\sum_{n=-\infty}^{\infty}s_n\cdot\exp\left[i\left(\frac{2\pi}{d}nx+\beta_n h\right)\right]\right\}$$
$$=\sum_{n=0}^{\infty}b_n\cos(B_n h)\cos\left[\frac{n\pi}{c}\left(x+\frac{c}{2}\right)\right]\cdot\exp(-i\alpha_0 x), \quad (16)$$

$$\cos^2\left\{-\beta_0\exp(-i\beta_0 h)+\sum_{n=-\infty}^{\infty}\beta_n s_n\cdot\exp\left[i\left(\frac{2\pi}{d}nx+\beta_n h\right)\right]\right\}$$
$$=\sum_{n=0}^{\infty}ib_n B_n\sin(B_n h)\cos\left[\frac{n\pi}{c}\left(x+\frac{c}{2}\right)\right]\cdot\exp(-i\alpha_0 x). \quad (17)$$

For $c/2 < |x| \le d/2$,

$$\cos^2\phi\left\{-\beta_0\exp(-i\beta_0 h)+\sum_{n=-\infty}^{\infty}\beta_n s_n\cdot\exp\left[i\left(\frac{2\pi}{d}nx+\beta_n h\right)\right]\right\}=0. \quad (18)$$

Similar to the fast polarization case, we have a dual series system derived from (16), (17), and (18) (Appendix II):

$$\sum_{n=-\infty}^{\infty}\zeta_n\exp(in\psi)=\sum_{n=-\infty}^{\infty}h_n\exp[i(n\nu-\tau)\psi],\qquad 0\le|\psi|<\psi_0 \quad (19)$$

$$\sum_{n=-\infty}^{\infty}\zeta_n\exp(in\psi)=0,\qquad \psi_0<|\psi|\le\pi \quad (20)$$

where

$$\zeta_0=-\beta_0\exp(-i\beta_0 h)+\beta_0 s_0\exp(i\beta_0 h)$$
$$\zeta_n=\beta_n s_n\exp(i\beta_n h),\qquad n\ne 0$$

$$h_n = \frac{(\delta_{n0}+1)B_n \tan (B_n h)}{2} \sum_{m=-\infty}^{\infty} \cdot \left[2\delta_{m0} \exp (-i\beta_0 h) + \frac{\zeta_m}{\beta_m}\right] t_{nm} \cdot \begin{cases} i, & |\alpha_m c| = n\pi \\ \dfrac{(2\alpha_m c)[(-1)^n \exp (i\alpha_m c) - 1]}{(\alpha_m c)^2 - (n\pi)^2}, & |\alpha_m c| \neq n\pi \end{cases}.$$

Equations (19) and (20) constitute the dual series problem for the slow-polarization case. The solution unknowns ζ_n, i.e., $n = 0, \pm 1, \pm 2, \cdots$, can be obtained with the Riemann-Hilbert problem techniques.

III. A Riemann-Hilbert Approach to the Dual Series Problem

By matching the tangential fields at the electromagnetic boundary, we derived the following dual series systems for the unknown coefficients in the previous sections: (14) and (15), for the fast polarization case, and (19) and (20) for the slow polarization case. In this section we apply the Riemann-Hilbert problem techniques to solve each of these dual series systems.

A. Fast Polarization Case

Differentiating (14) with respect to ψ and substituting $x_m = m\eta_m$, $(m \neq 0)$, in (14) and (15), we obtain the following equations:

$$\sum_{\substack{n=-\infty \\ n\neq 0}}^{\infty} x_n \exp (in\psi) = 0, \qquad \psi_0 < |\psi| \leq \pi. \tag{21}$$

$$\sum_{\substack{n=-\infty \\ n\neq 0}}^{\infty} x_n \frac{|n|}{n} \exp (in\psi) = \xi\eta_0 + \sum_{m=-\infty}^{\infty} f_m \exp (im\psi) + \sum_{n=-\infty}^{\infty} g_n \exp [i(n\nu - \tau)\psi], \qquad 0 \leq |\psi| < \psi_0. \tag{22}$$

With the condition

$$-\eta_0 = \sum_{\substack{n=-\infty \\ n\neq 0}}^{\infty} \frac{x_n}{n} \exp (in\psi),$$

two functions are introduced

$$X_+(z) = \sum_{m>0} x_m z^m, \quad X_-(z) = -\sum_{m<0} x_m z^m.$$

We assume that x_+ and x_- are analytic functions on the interior and exterior of the unit circle S (Fig. 9), respectively. Rewrite (21) and (22) as

$$X_+(z) - X_-(z) = 0, \qquad z \in L = \{\exp (i\psi) | \psi_0 < |\psi| \leq \pi\} \tag{23a}$$

$$X_+(z) - T(z)X_-(z) = F(z), \qquad z \in \Gamma = \{\exp (i\psi) | 0 \leq |\psi| < \psi_0\} \tag{23b}$$

where

$$T(z) = -1 \text{ and } F(z) = \xi\eta_0 + \sum_{m=-\infty}^{\infty} f_m z^m + \sum_{n=-\infty}^{\infty} g_n z^{(n\nu-\tau)}, \qquad \text{for } z \in \Gamma.$$

Then let

$$T_0(z) = \begin{cases} T(z), & z \in \Gamma \\ 1, & z \in L \end{cases}$$

$$F_0(z) = \begin{cases} F(z), & z \in \Gamma \\ 0, & z \in L \end{cases}.$$

An imhomogeneous Riemann-Hilbert problem [11] with a discontinuous coefficient $T_0(z)$ and a multivalued forcing function $F_0(z)$ is defined by (23a) and (23b):

$$X_+(z) - T_0(z)X_-(z) = F_0(z), \qquad z \in S(=\Gamma + L). \tag{24}$$

Riemann-Hilbert problems treated in the literature [6]-[10] involved only a single-valued forcing function. Since the number $(n\nu - \tau)$, the exponent of z in the above series $F(z)$, is not necessarily an integer, the function in our case $F(z)$ has a branch point at the origin and becomes multivalued in the complex variable z-plane. This multivalued forcing function is responsible for the edge behavior of the field function [9].

The problem formulated in (24) is reduced to one with continuous coefficients by introducing the characteristic function $(1/G(z))$, which has the same singular behavior as $X(z)$ at $\psi = \pm\psi_0$. That is

$$\frac{1}{G_+(z)} = T_0(z) \frac{1}{G_-(z)}, \qquad z \in S \tag{25}$$

where

$$G(z) = \begin{cases} G_+(z), & |z| < 1 \\ G_-(z), & |z| > 1 \end{cases}.$$

Multiplying (24) by $G_+(z)$, we obtain

$$\Phi_+(z) = \Phi_-(z) + \Psi(z), \qquad z \in S \tag{26}$$

where

$$\Phi(z) = G(z)X(z), \quad \Psi(z) = G_+(z)F_0(z),$$

$$\Phi_+(z) = \lim_{\substack{z\to S \\ |z|<1}} \Phi(z), \quad \Phi_-(z) = \lim_{\substack{z\to S \\ |z|>1}} \Phi(z).$$

Equation (26) represents the transition condition of a Riemann-Hilbert problem with continuous coefficients defined on the unit circle S. The solution given by Gakhov [11,

TABLE I
DEFINITION OF SOME IMPORTANT PARAMETERS THAT HAVE BEEN DERIVED IN APPENDIX IV

Variables	Index*		Closed form expression**
R_m	m (any integer)		$\left[\frac{1}{2}\right]P_m(\sigma)$
W^r	r = 0		$\left[\frac{1+\sigma}{2}\right]\ln\left[\frac{1+\sigma}{2}\right]$
	r ≠ 0		$-\frac{1}{2}\sin(\phi_0)P_r^{-1}(\sigma)\ln\left[\frac{1+\sigma}{2}\right]+\frac{1}{2r}[P_r(\sigma)-P_{r-1}(\sigma)]$
V_m^r	m ≠ r		$\frac{1}{2}\left[\frac{m+1}{m-r}\right][P_m(\sigma)P_{r+1}(\sigma)-P_{m+1}(\sigma)P_r(\sigma)]$
	m = r	m = r ≥ 0	$\frac{m+1}{2}[P_{m+1}(\sigma)U_m(\sigma)-P_m(\sigma)U_{m+1}(\sigma)]$
		m = r = −1	0
		m = r ≤ −2	$\frac{m+1}{2}[P_{-m-1}(\sigma)U_{-m-2}(\sigma)-P_{-m-2}(\sigma)U_{-m-1}(\sigma)]$
Y	no index		$\left[-\frac{1}{2}\right]\ln\left[\frac{1+\sigma}{2}\right]$

* r is a real number and m is an integer.

** $\sigma=\cos(\phi_0)$ and $\phi_0=\frac{c\pi}{d}$.

pp. 96–99] is

$$\Phi(z)=\frac{1}{2\pi i}\int_S\frac{\Psi(\lambda)}{\lambda-z}\,d\lambda+c_0,\qquad\text{where } c_0 \text{ is a constant.}$$

Consequently, the desired solution of (24) is defined as

$$X(z)=\frac{1}{2\pi i}\frac{1}{G(z)}\int_\Gamma\frac{G_+(\lambda)F(\lambda)}{\lambda-z}\,d\lambda+\frac{c_0}{G(z)}. \tag{27}$$

The characteristic function $G(z)$ is also given by Gakhov [11, p. 424];

$$G(z)=\sqrt{(z-\alpha)(z-\bar{\alpha})},$$

where $\alpha=\exp(i\psi_0)$ and $\bar{\alpha}=\exp(-i\psi_0)$.

From (26), (27) and the Plemelj–Sokhotskii conditions [11] (Appendix III),

$$\begin{aligned}&X_+(z)+T(z)X_-(z)\\&=\frac{2}{G_+(z)}\left[\frac{1}{2\pi i}\int_\Gamma\frac{G_+(\lambda)F(\lambda)}{\lambda-z}\,d\lambda+c_0\right]\\&=X_+(z)-X_-(z)=\sum_{\substack{m=-\infty\\m\neq0}}^{\infty}x_m\exp(im\psi),\qquad z\in\Gamma.\end{aligned} \tag{28}$$

Fourier inversion of (28) then yields as follows.

(1) $m \neq 0$

$$x_m=\frac{1}{2\pi}\int_{-\psi_0}^{\psi_0}\left\{\frac{2}{G_+(e^{i\psi})}\left[\frac{1}{2\pi i}\cdot\int_\Gamma\frac{G_+(\lambda)F(\lambda)}{\lambda-e^{i\psi}}\,d\lambda+c_0\right]\right\}e^{im\psi}\,d\psi.$$

Substituting $F(\lambda)$ from (23b) into the above equation gives;

$$x_m=v_m^0\xi\eta_0+\sum_{n=-\infty}^{\infty}v_m^nf_n+\sum_{n=-\infty}^{\infty}v_m^{(n\nu-\tau)}g_n+2R_mc_0, \tag{29a}$$

where

$$v_m^r=\frac{1}{2\pi}\int_{-\psi_0}^{\psi_0}\frac{e^{-im\psi}}{G_+(e^{i\psi})}\left[\frac{1}{\pi i}\int_\Gamma\frac{G_+(\lambda)\lambda^r}{\lambda-e^{i\psi}}\,d\lambda\right]d\psi,$$

$$R_m=\frac{1}{2\pi}\int_{-\psi_0}^{\psi_0}\frac{e^{-im\psi}}{G_+(e^{i\psi})}\,d\psi.$$

Closed-form representations for v_m^r and R_m are given in Table I. The proofs are given in Appendix IV.

(2) $m = 0$

$$0=v_0^0\xi\eta_0+\sum_{n=-\infty}^{\infty}v_0^nf_n+\sum_{n=-\infty}^{\infty}v_0^{(n\nu-\tau)}g_n+2R_0c_0. \tag{29b}$$

Now impose the auxiliary condition:

$$-\eta_0=\sum_{\substack{n=-\infty\\n\neq0}}^{\infty}\frac{x_n}{n}\exp(in\psi),\qquad\psi_0<|\psi|\le\pi.$$

We substitute x_n obtained in (29a) and let $\psi = \pi$ to give

$$-\eta_0 = w^0 \xi \eta_0 + \sum_{n=-\infty}^{\infty} w^n f_n + \sum_{n=-\infty}^{\infty} w^{(n\nu-\tau)} g_n + 2Yc_0, \quad (29c)$$

where

$$w^r = \sum_{\substack{m=-\infty \\ m\neq 0}}^{\infty} \frac{v_m^r (-1)^m}{m}, \quad Y = \sum_{\substack{m=-\infty \\ m\neq 0}}^{\infty} \frac{R_m (-1)^m}{m}.$$

Closed-form representations of w^r and Y are given in Table I, and the proofs are given in Appendix IV.

Equations (29a), (29b), and (29c) constitute an infinite system of linear equations. We truncate the infinite series in each equation at some value N and use Gauss elimination to solve the remaining finite system for the unknowns c_0, η_0, $\eta_{\pm 1}$, $\cdots$, $\eta_{\pm N}$. Typically, reasonable convergence is achieved with $N \geq 100\ d/\lambda$ [9], where the coefficients of x_n(or $n\eta_n$), $n > N$, in the right-hand side of (29a)–(29c) are negligible.

B. Slow Polarization Case

Consider the dual series problem, (19) and (20), presented in Section II-C:

$$\sum_{n=-\infty}^{\infty} \zeta_n \exp(in\psi) = \sum_{n=-\infty}^{\infty} h_n \exp[i(n\nu-\tau)\psi], \quad 0 \leq |\psi| < \psi_0 \quad (19)$$

$$\sum_{n=-\infty}^{\infty} \zeta_n \exp(in\psi) = 0, \quad \psi_0 < |\psi| \leq \pi. \quad (20)$$

It can be reduced to a Riemann–Hilbert problem as follows. Introduce the functions:

$$Y_+(z) = \sum_{m\geq 0} \zeta_m z^m, \quad Y_-(z) = -\sum_{m<0} \zeta_m z^m.$$

Assume Y_+ and Y_- are analytic on the interior and exterior of the unit circle S, respectively. Rewrite (19) and (20) as

$$Y_+(z) - Y_-(z) = 0, \quad z \in L = \{\exp(i\psi) | \psi_0 < |\psi| \leq \pi\} \quad (30a)$$

$$Y_+(z) - Y_-(z) = H(z), \quad z \in \Gamma = \{\exp(i\psi) | 0 \leq |\psi| < \psi_0\} \quad (30b)$$

where

$$H(z) = \sum_{n=-\infty}^{\infty} h_n z^{(n\nu-\tau)}, \quad \text{for } z \in \Gamma.$$

Equations (30a), (30b) are analogous to (23a), (23b) except that $T(z) = 1$ rather than -1 as in the fast polarization case. Following the same procedures as in the fast polarization case, we formulate a Riemann–Hilbert problem with continuous coefficients. The characteristic function $(1/G(z))$ is now defined as [11]

$$G(z) = \sqrt{|(z-\alpha)(z-\bar{\alpha})|},$$

where $\alpha = \exp(i\psi_0)$ and $\bar{\alpha} = \exp(-i\psi_0)$.

Similar to (28) one can easily obtain the following equation:

$$Y_+(z) - Y_-(z) = \sum_{n=-\infty}^{\infty} \zeta_n \exp(in\psi) = H(z), \quad z \in \Gamma. \quad (31)$$

Fourier inversion of this expression gives the terms

$$\zeta_m = \sum_{n=-\infty}^{\infty} h_n \bar{Q}_{mn}, \quad \text{for all } m \quad (32)$$

where

$$\bar{Q}_{mn} = \frac{1}{2\pi} \int_\Gamma \exp[i(n\nu-\tau-m)\psi]\, d\psi = \frac{\psi_0}{\pi} \operatorname{sinc}[(n\nu-\tau-m)\psi_0].$$

Equations (32) constitute an infinite system of linear equations with unknown variables ζ_0, $\zeta_{\pm 1}$, $\zeta \pm 2$, $\cdots$. We truncate the infinite series at some value N and use Gauss elimination to solve the remaining finite system of equations. The value of N is chosen to be $N \geq 100\ d/\lambda$ so that the coefficients ζ_m associated with the forcing terms, $h_n \bar{Q}_{mn}$ where $n > N$ or $m > N$, in (32) are negligible and the convergence of the solution is obtained [9].

IV. Numerical Results and Conclusions

The theoretical results developed with the Riemann–Hilbert techniques were implemented as Fortran programs. We simulated the diffraction processes and computed both the diffraction efficiencies and the phase differences for arbitrary wave incident angles.

The nth order diffraction efficiency [2] is defined as the ratio of the real power carried by the nth diffracted wave in the direction normal (y-axis direction in Fig. 1) to the plane boundary to the real power associated with the incident wave in the same normal direction (i.e., y-axis direction). It is calculated by

$$er_n = |r_n|^2 \frac{\cos\theta_n}{\sin\theta}, \quad \text{for the fast polarization case.}$$

$$es_n = |s_n|^2 \frac{\cos\theta_n}{\sin\theta}, \quad \text{for the slow polarization case}$$

where $\theta_n = \sin^{-1}(\alpha_n/k\cos\phi)$. On the other hand, the phase differences between the incident plane wave and the zero-order diffracted wave are computed by the following formulas [5]:

$$pr_0 = \arg[r_0 \exp(2i\beta_0 h)], \quad \text{for the fast polarization case.}$$

$$ps_0 = \arg[-s_0 \exp(2i\beta_0 h)], \quad \text{for the slow polarization case.}$$

The diffraction problem of our particular interest is when the ratio of the grating period to the incident wavelength falls in the neighborhood of 0.25. Studies [1], [5] showed that the polarization direction of the zero-order diffracted wave is controllable by the groove depth h in this region. The mechanism [5] mainly depends on the relative phases of two orthogonal polarizations as defined above. In this section we will derive the analytical formulae for the phase value calculations so that hypothesis and conventional wisdom found in the literature are strictly verified.

Based on the Riemann–Hilbert method, the contour plots of the magnitude of two tangential field components near the aperture were generated in Figs. 3(a), 3(c) and Figs. 4(a), 4(c) where the series truncation number N was taken to be 100. We also plotted the fields magnitude at $y = h$ (the interface between region 1 and 2 defined in Section II-A) in Figs. 3(b), 3(d) and 4(b), 4(d). The electric fields in Figs. 3(a), 3(b) and 4(a), 4(b) drop to zero on the metallic surface within an error less than 3 percent. Discontinuities at the groove edges are found in the plots for $|H_x|$ in the fast polarization case and for $|E_x|$ in the slow polarization case. These results checked the underlying theories, the boundary conditions, and our computer programs.

For the cases to be discussed below, the grating dimensions were expressed in terms of the ratios: $d/\lambda = 0.25$, $d/c = 2$, where d is the groove period, c is the groove width and λ is the incident wavelength. The groove depth h was varied from 0.01 λ to 0.30 λ. Convergence of the solutions of the linear systems is easily achieved with a series truncation number $N = 16$. As expected, the mode-matching method [5] predicts the zero order diffraction efficiencies er_0 and es_0 to be 100 percent at all incident angles. The phase differences between the two orthogonal polarizations ($pr_0 - ps_0$) are plotted in Fig. 5 for the fixed incident angles, $\phi = 0°$ and $\theta = 90°$. Results generated with the Riemann–Hilbert approach, mode-matching method [5] and the iteration method [1] are given. We see that the Riemann–Hilbert method reproduces the mode-matching method results while the iteration method tends to diverge when the groove depth h approaches one-quarter wavelength.

We change the ratios of d/c to 2.5 and recompute the phase differences ($pr_0 - ps_0$). Fig. 6(a) shows that the mode-matching method produces wiggly curves. The zigzag shape of the curves demonstrates that this method fails to track the correct phase variations. On the other hand, the Riemann–Hilbert method (Fig. 6(b)) generates smooth curves and is believed to be a numerically stable approach in this region. There are nine curves given in each of the figures, representing nine values of the incident angle $\theta (0° \le \theta \le 90°)$. As will be discussed later, these nine curves intersect at a common point where $pr_0 - ps_0 = 180°$ and $h \approx 0.25\ \lambda$.

We continued to make the groove width c of the grating smaller and smaller while keeping all the other parameters fixed. The solutions for the phase differences are shown in Figs. 7(a)–7(d). We observe that in Fig. 7(d) all the curves, independent of the incident angles, converge into one that attains a $2\pi n$ phase difference between these two orthogonally polarized waves, where n is an integer. This limiting case is the simple problem of the reflection of electromagnetic waves by a smoothly polished, perfectly conducting plane. Each of the reflected waves is 180° out of phase with its own incident wave. Consequently, the phase difference between these two reflected waves is an integer multiple of 360°.

We also computed each of the quantities pr_0 and ps_0 as a function of the groove width c keeping the groove depth h fixed (Figs. 8(a)–8(d)). We see that pr_0 decreases slightly from 180° when c increases from zero. This modifies the conventional wisdom that the fast polarized wave reflects from the top surfaces of the grooves and experiences a 180° phase difference [1]. If we make the groove depth h smaller and smaller, all the curves for both the fast and the slow polarization cases flatten out and tend to converge into one (Fig. 8(d) that returns to the previous case in which no grooves exist.

In order to better understand the nonlinearity associated with the quantity ($pr_0 - ps_0$), we truncate the infinite systems of (29) at $N = 1$ and at $N = 0$ for (32). We obtain the following analytical results:

$$r_0 \exp(2i\beta_0 h) = \frac{\ln\left(\frac{1+\cos\psi_0}{2}\right) + i\frac{2\pi}{d\beta_0}G_f}{\ln\left(\frac{1+\cos\psi_0}{2}\right) - i\frac{2\pi}{d\beta_0}G_f}, \tag{33}$$

where

$$G_f = 1 + 2dA_1 \cot(A_1 h)\left[\frac{\sin\left(\frac{\alpha_0 c+\pi}{2}\right)}{\pi^2-(\alpha_0 c)^2}\right] \cdot [(w^{-\nu-\tau}-w^{\nu-\tau})R_0 + (v_0^{\nu-\tau}-v_0^{-\nu-\tau})Y] + dA_1 \cot(A_1 h) \cdot \left[\frac{\sin\left(\frac{\alpha_1 c+\pi}{2}\right)}{\pi^2-(\alpha_1 c)^2}\cos\psi_0 - \frac{\sin\left(\frac{\alpha_{-1} c+\pi}{2}\right)}{\pi^2-(\alpha_{-1} c)^2}\right] \cdot (v_0^{-\nu-\tau}-v_0^{\nu-\tau})$$

and

$$-s_0 \exp(2i\beta_0 h) = -\frac{\beta_0 + i\frac{2c}{d}B_0 \tan(B_0 h)\left[\operatorname{sinc}\left(\frac{\alpha_0 c}{2}\right)\right]^2}{\beta_0 - i\frac{2c}{d}B_0 \tan(B_0 h)\left[\operatorname{sinc}\left(\frac{\alpha_0 c}{2}\right)\right]^2}. \tag{34}$$

Let $pr_0 - ps_0 = 180°$. Then from (33) and (34) we obtain

$$\tan(B_0 h) = \frac{\lambda |G_f|}{\cos\phi(2c)\left[\operatorname{sinc}\left(\frac{\alpha_0 c}{2}\right)\right]^2 \left|\ln\left(\frac{1+\cos\psi_0}{2}\right)\right|}. \tag{35}$$

This equation shows the relationship among the relevant parameters when the relative phase difference equals 180 degrees (i.e., $pr_0 - ps_0 = 180°$). Note that if we substitute c

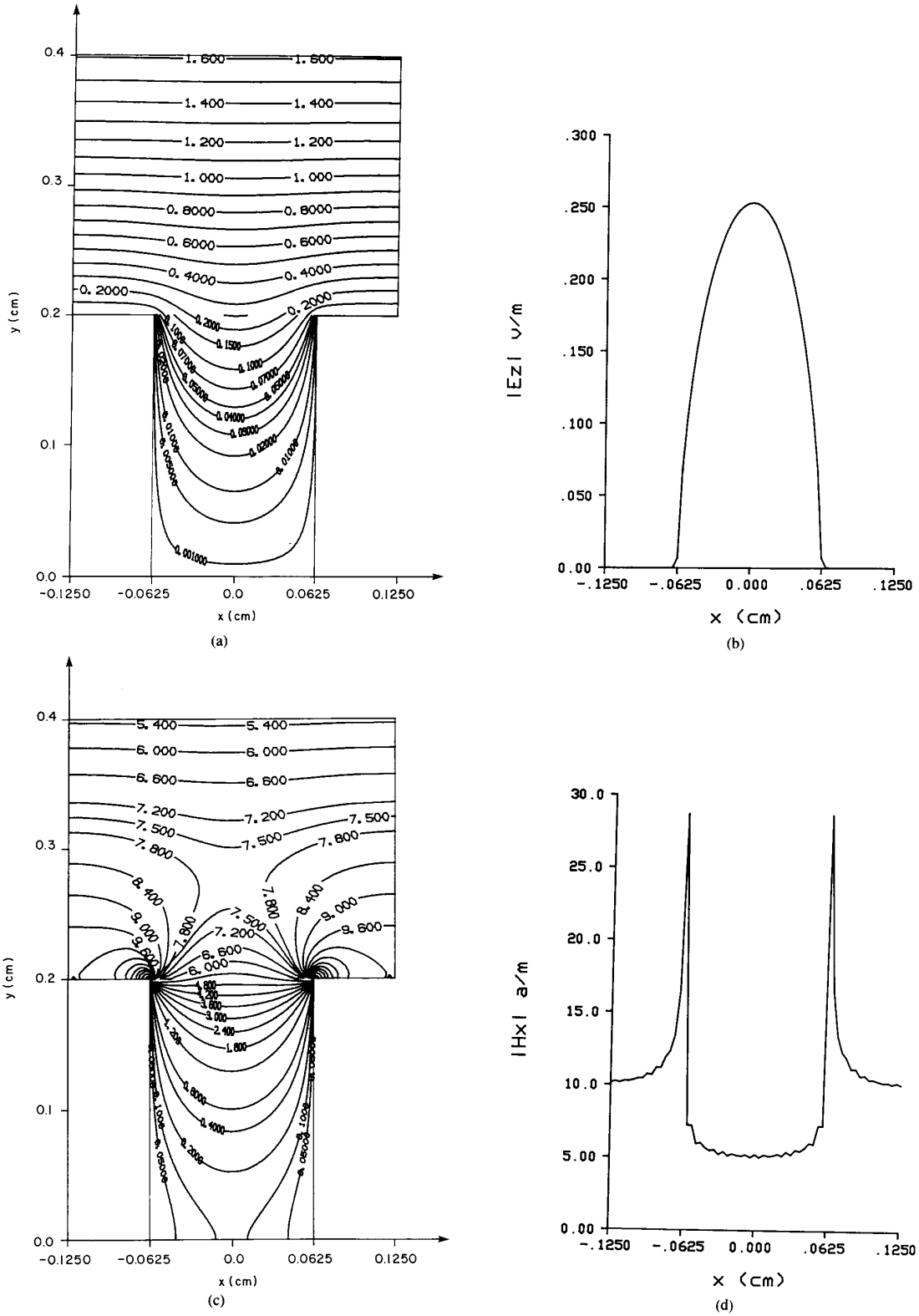

Fig. 3. The Riemann–Hilbert approach produces the magnitude of some field components generated by the fast polarized incident wave. The parameters are: $\lambda = 1$ cm, $d = 0.25$ cm, $d/c = 2$, $h = 0.2$ cm, $\theta = 45°$, $\phi = 0°$. (a) Contour plots of the magnitude of the electric field component $|E_z|$. (b) At $y = h = 0.2$ cm, $|E_z|$ is plotted as a function of the x coordinate. (c) Contour plots of the magnitude of the electric field component $|H_x|$. (d) At $y = h = 0.2$ cm, $|H_x|$ is plotted as a function of the x coordinate.

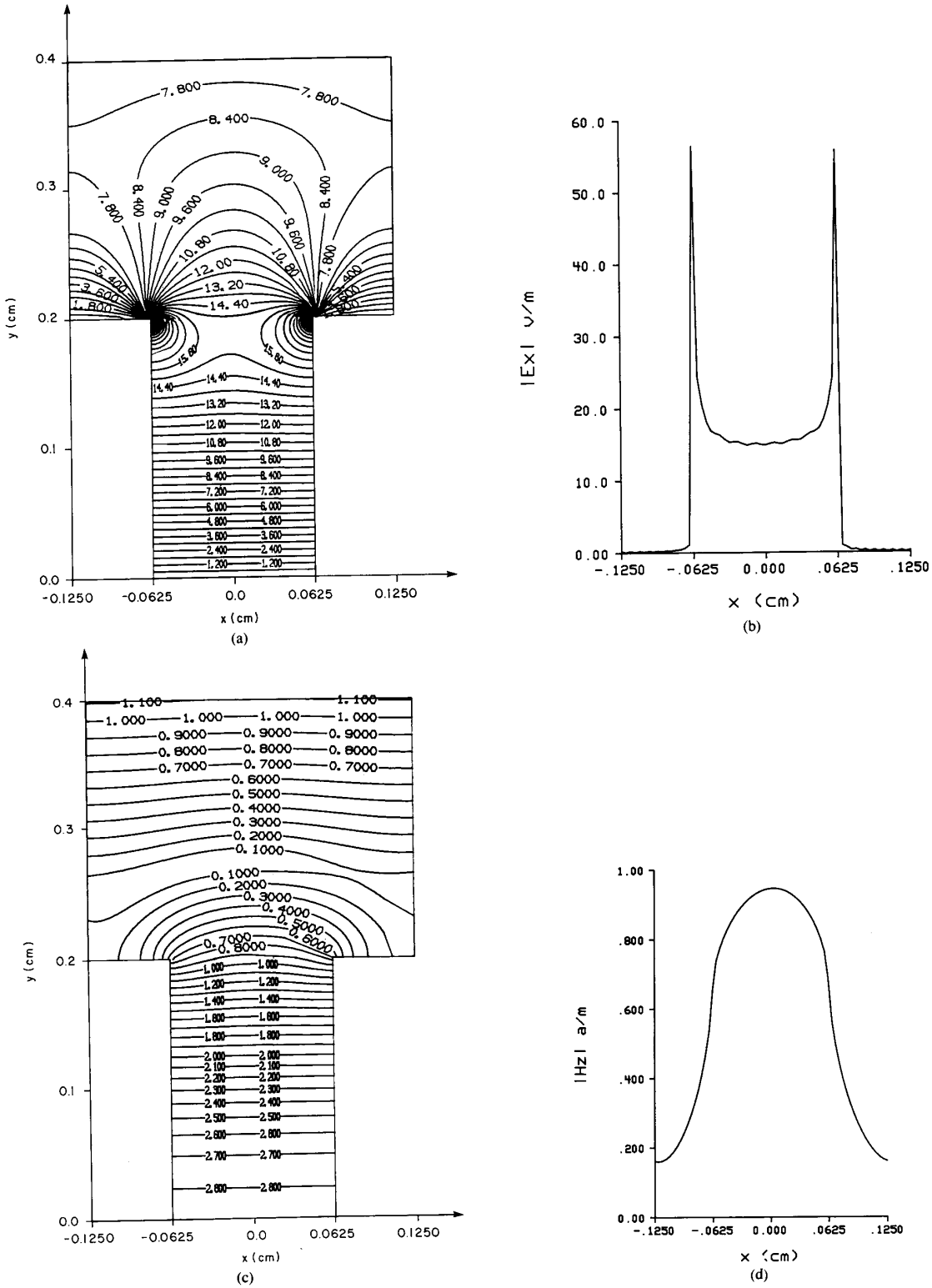

Fig. 4. The Riemann–Hilbert approach produces the mangitude of some field components generated by the slow polarized incident wave. The parameters are: $\lambda = 1$ cm, $d = 0.25$ cm, $d/c = 2$, $h = 0.2$ cm, $\theta = 45°$, $\phi = 0°$. (a) Contour plots of the magnitude of the electric field component $|E_x|$. (b) At $y = h = 0.2$ cm, $|E_x|$ is plotted as a function of the x coordinate. (c) Contour plots of the magnitude of the electric field component $|H_z|$. (d) At $y = h = 0.2$ cm, $|H_z|$ is plotted as a function of the x coordinate.

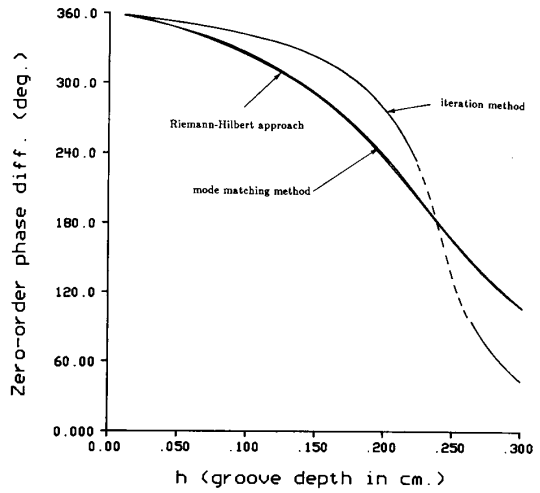

Fig. 5. A comparison among the results from the iteration method, the mode-matching method and the Riemann-Hilbert approach. The phase differences ($pr_0 - ps_0$) between two orthogonal polarizations are plotted as a function of the groove depth h. When the phase difference approaches 180°, the iteration method begins to diverge (dash line portion) from the correct result. Results from the Riemann-Hilbert approach coincide with mode-matching solution. The parameters are: $\lambda = 1$ cm, $d = 0.25$ cm, $d/c = 2$, $\theta = 90°$, $\phi = 0°$.

$= 0$, then for $|G_f| > 0$ (35) reduces to

$$h = \frac{\pi/2}{B_0} = \frac{\lambda}{4 \cos \phi}. \tag{36}$$

This result was hypothesized by Kok and Gallagher [5] but was not derived directly from the mode-matching solution. If we substitute $c = d/2 = \lambda/8$ and let $|G_f| = 2$ for $\phi = 0°$, $\theta = 90°$, we have $h = 0.236\ \lambda$ from (35). This explains why the common intersection in Figs. 6(b) and Figs. 7(a)-7(d) is slightly offset from $h = 0.25\ \lambda$.

In conclusion, we found (Figs. 5 and 6(a)) that purely numerical methods (i.e., the iteration and the mode-matching methods) may encounter difficulties. This is due to the discontinuous behavior of the field functions at the groove edges (see Figs. 3(c), 3(d) and 4(a), 4(b)). The Riemann-Hilbert approach, however, provides an effective way of solving this class of grating problems. It formulates the grating problem as a boundary value problem in complex variable theory. The singular nature of the electromagnetic problem is analytically resolved with the Riemann-Hilbert problem techniques. Once the equivalent boundary value problem is solved, one can easily achieve convergence of the numerical calculations for the modal coefficients and for the subsequent field functions. Results generated with the Riemann-Hilbert approach to the dual series equations show that this method works well for arbitrary incident angles, wavelengths, and for any groove dimension.

Appendix I

Let

$$\eta_n = \begin{cases} \exp(-i\beta_0 h) + r_0 \exp(i\beta_0 h), & n = 0 \\ r_n \exp(i\beta_n h), & n \neq 0. \end{cases}$$

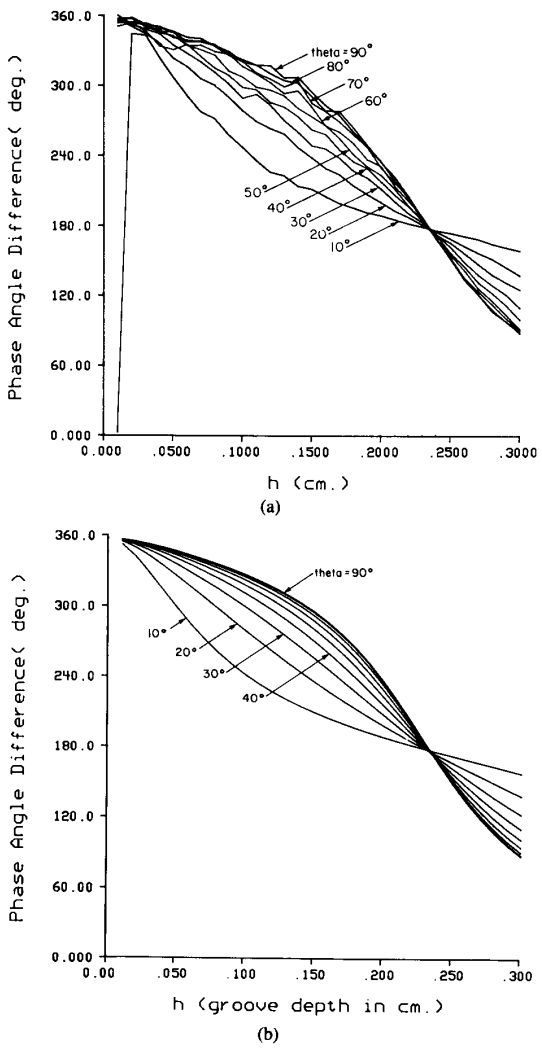

Fig. 6. (a) The phase differences ($pr_0 - ps_0$) obtained by the mode-matching method appear unstable for the parameters: $\lambda = 1$ cm, $d = 0.25$ cm, $d/c = 2.5$, $0 < h < 0.30$ cm, $\phi = 0°$, $10° \leq \theta \leq 90°$. (b) The phase difference ($pr_0 - ps_0$) obtained by the Riemann-Hilbert approach are stable for the parameters: $\lambda = 1$ cm, $d = 0.25$ cm, $d/c = 2.5$, $0 < h \leq 0.30$ cm, $\phi = 0°$, $10° \leq \theta \leq 90°$.

Then (13) can be written as

$$\sum_{n=-\infty}^{\infty} \eta_n \exp\left(in \frac{2\pi x}{d}\right) = 0, \qquad \frac{c\pi}{d} < \left|\frac{2\pi x}{d}\right| \leq \pi. \tag{37}$$

Let $\psi_0 = \pi c/d$, $\psi = 2\pi x/d$, then (14) in Section II-C is obtained from (37).

Rewrite (11), (12) as

$$\sum_{n=-\infty}^{\infty} \eta_n \exp(i\alpha_n x) = \sum_{n=1}^{\infty} a_n \sin(A_n h) \cdot \sin\left[\frac{n\pi}{c}\left(x + \frac{c}{2}\right)\right] \Big/ \cos^2 \phi, \tag{38}$$

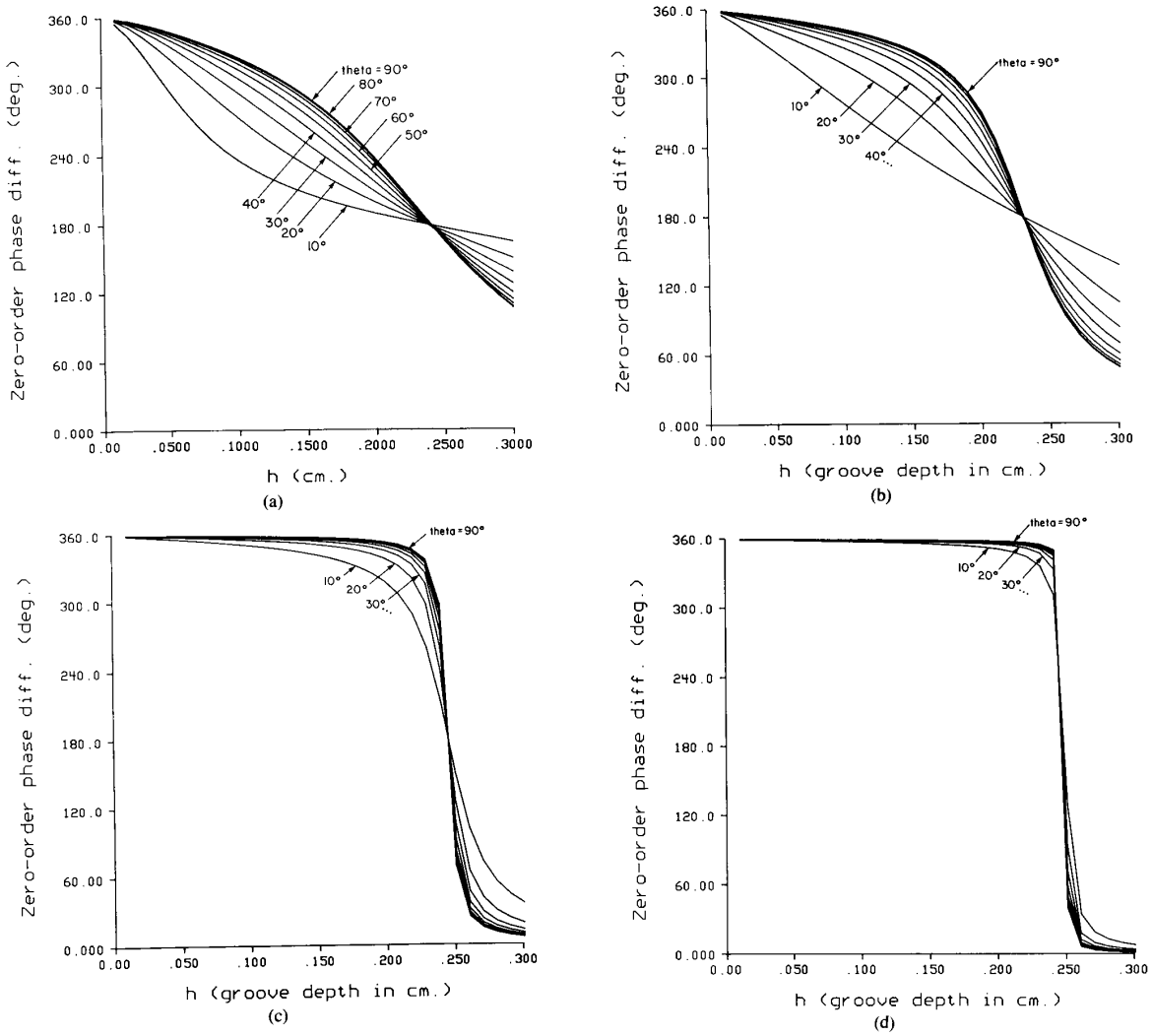

Fig. 7. (a) The phase difference ($pr_0 - ps_0$) versus the groove depth h. $\lambda = 1$ cm, $d = 0.25$ cm, $d/c = 2$, $\phi = 0°$, $10° \le \theta \le 90°$. (b) The phase difference ($pr_0 - ps_0$) versus the groove depth h. $\lambda = 1$ cm, $d = 0.25$ cm, $d/c = 5$, $\phi = 0°$, $10° \le \theta \le 90°$. (c) The phase difference ($pr_0 - ps_0$) versus the groove depth h. $\lambda = 1$ cm, $d = 0.25$ cm, $d/c = 50$, $\phi = 0°$, $10° \le \theta \le 90°$. (d) The phase difference ($pr_0 - ps_0$) versus the groove depth h. $\lambda = 1$ cm, $d = 0.25$ cm, $d/c = 250$, $\phi = 0°$, $10° \le \theta \le 90°$.

$$\sum_{n=-\infty}^{\infty} i\eta_n\beta_n \exp(i\alpha_n x) - 2i\beta_0 \exp[i(\alpha_0 x - \beta_0 h)] = \sum_{n=1}^{\infty} a_n A_n \cos(A_n h) \sin\left[\frac{n\pi}{c}\left(x+\frac{c}{2}\right)\right] \Big/ \cos^2\phi. \quad (39)$$

Compute the Fourier sine series coefficients a_n in (38) and then substitute them into (39). We have

$$\sum_{\substack{n=-\infty \\ n\neq 0}}^{\infty} \eta_n\beta_n \exp\left(i\frac{2\pi x}{d}n\right) = -\eta_0\beta_0 + 2\beta_0 \exp(-i\beta_0 h) + \sum_{n=1}^{\infty} A_n \cot(A_n h).$$

$$\sum_{m=-\infty}^{\infty} \eta_m \sin\left[\frac{n\pi}{c}\left(x+\frac{c}{2}\right)\right] \exp(-i\alpha_0 x) S1_{nm}, \quad (40)$$

where

$$S1_{nm} = \begin{cases} \mp i \exp(-i\alpha_m c/2), & \text{if } \alpha_m c = \pm n\pi. \\ \exp(-i\alpha_m c/2) \dfrac{(-2n\pi)[(-1)^n \exp(i\alpha_m c) - 1]}{(\alpha_m c)^2 - (n\pi)^2}, & \text{if } \alpha_m c \neq \pm n\pi. \end{cases}$$

Substituting

$$\beta_n = \sqrt{k^2 - \gamma^2 - \alpha_n^2} = \frac{2\pi|n|i}{d}\left[\left(\frac{\alpha_0 d}{2\pi n}+1\right)^2 - \left(\frac{d\hbar}{2\pi n}\right)^2\right]^{1/2} = \frac{2\pi|n|i}{d}(1-\epsilon_n),$$

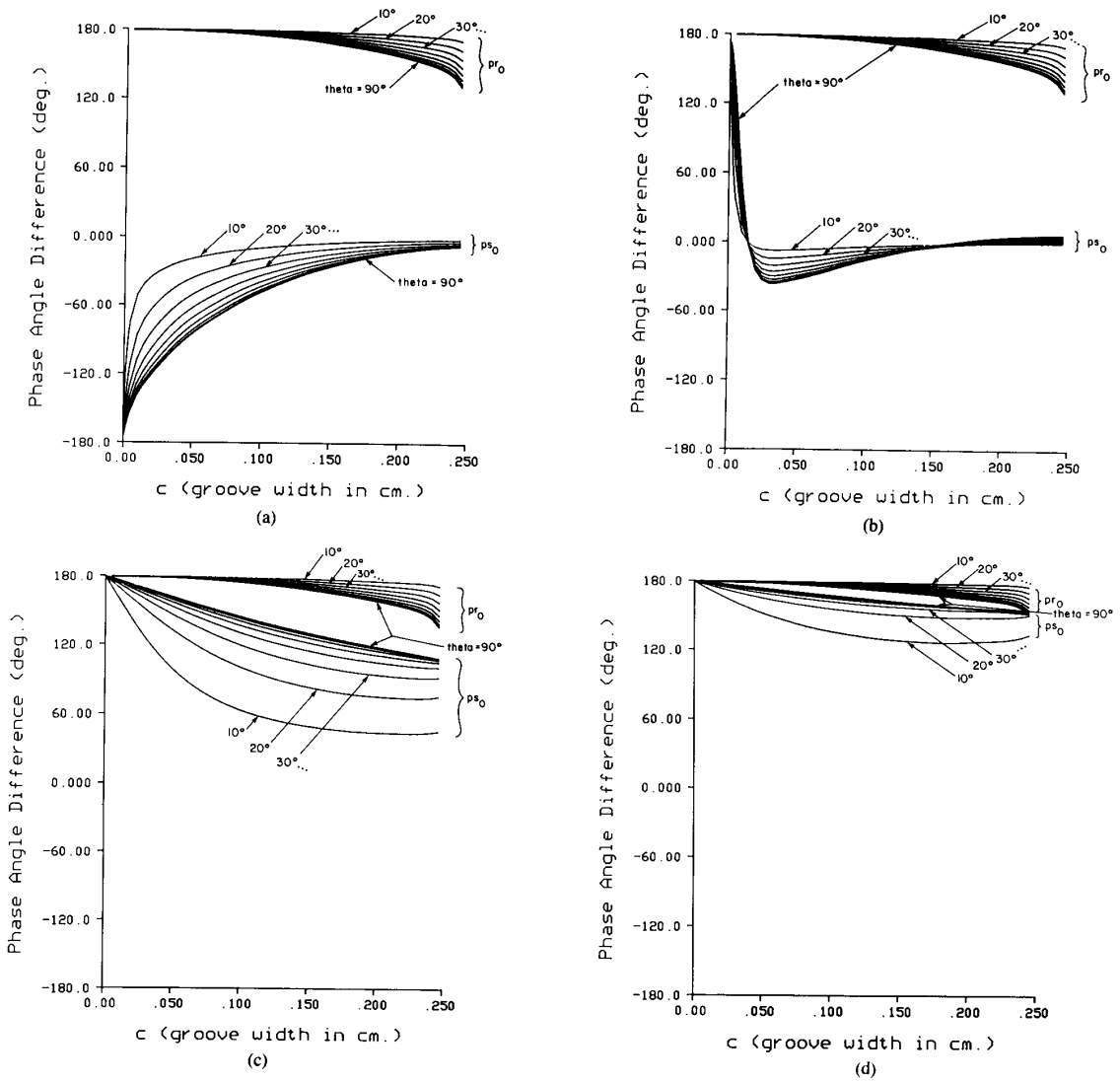

Fig. 8. (a) The phase differences, pr_0 and pr_0, versus the groove width c. $\lambda = 1$ cm, $d = 0.25$ cm, $h = 0.26$ cm, $\phi = 0°$, $10° \leq \theta \leq 90°$. (b) The phase differences, pr_0 and ps_0, versus the groove width c. $\lambda = 1$ cm, $d = 0.25$ cm, $h = 0.24$ cm, $\phi = 0°$, $10° \leq \theta \leq 90°$. (c) The phase differences, pr_0 and ps_0, versus the groove width c. $\lambda = 1$ cm, $d = 0.25$ cm, $h = 0.1$ cm, $\phi = 0°$, $10° \leq \theta \leq 90°$. (d) The phase differences, pr_0 and ps_0, versus the groove width c. $\lambda = 1$ cm, $d = 0.25$ cm, $h = 0.04$ cm, $\phi = 0°$, $10° \leq \theta \leq 90°$.

and

$$\psi = \frac{2\pi x}{d}, \quad \psi_0 = \frac{c\pi}{d}, \quad \text{and} \quad \nu = \frac{d}{2c}, \quad \tau = \frac{\alpha_0 d}{2\pi},$$

into (40), (15) in Section II-C follows immediately.

Appendix II

Let

$$\zeta_n = \begin{cases} -\beta_0 \exp(-i\beta_0 h) + \beta_0 s_0 \exp(i\beta_0 h), & n = 0 \\ \beta_n s_n \exp(i\beta_n h), & n \neq 0. \end{cases}$$

Then (18) can be written as

$$\sum_{n=-\infty}^{\infty} \zeta_n \exp\left(i \frac{2\pi n}{d} x\right) = 0, \qquad c/2 < |x| \leq d/2. \quad (41)$$

Equation (20) in Section II-C can be obtained from (41). Rewrite (16), (17) as

$$\sum_{n=-\infty}^{\infty} \left[\frac{\zeta_n}{\beta_n} + \delta_{n0} 2 \exp(-i\beta_0 h)\right] \exp(i\alpha_n x) = \sum_{n=0}^{\infty} b_n \frac{\cos(B_n h)}{\cos^2 \phi} \cos\left[\frac{n\pi}{c}\left(x + \frac{c}{2}\right)\right], \quad (42)$$

$$\sum_{n=-\infty}^{\infty} \zeta_n \exp(i\alpha_n x) = \sum_{n=0}^{\infty} ib_n \frac{B_n \sin(B_n h)}{\cos^2 \phi} \cdot \cos\left[\frac{n\pi}{c}\left(x + \frac{c}{2}\right)\right]. \quad (43)$$

Compute the Fourier cosine series coefficients in (42) and then substitute them into (43). We have

$$\sum_{n=-\infty}^{\infty} \zeta_n \exp\left(i\frac{2\pi}{d}nx\right) = \sum_{n=0}^{\infty} B_n \tan(B_n h) \sum_{m=-\infty}^{\infty} \left[\frac{\zeta_m}{\beta_m} + \delta_{m0} 2 \exp(-i\beta_0 h)\right] \cdot S2_{nm} \cos\left[\frac{n\pi}{c}\left(x+\frac{c}{2}\right)\right] \exp(-i\alpha_0 x), \quad (44)$$

where

$$S2_{nm} = \begin{cases} i \exp(-i\alpha_m c/2), & |\alpha_m c| = |n\pi| \\ \exp(-i\alpha_m c/2) \dfrac{(2\alpha_m c)[(-1)^n \exp(i\alpha_m c) - 1]}{(\alpha_m c)^2 - (n\pi)^2}, & |\alpha_m c| \neq |n\pi|. \end{cases}$$

Equation (44) can be easily simplified into (19) with a change of variables.

Appendix III

The Plemelj-Sokhotskii Conditions and the Riemann-Hilbert Problem

Suppose that one is given a simple, closed, smooth curve Γ dividing the complex plane into two open sets, the (bounded) interior S_+ and the exterior S_- and two Hölder continuous functions of position on that contour, $T(\gamma)$ and $F(\gamma)$, $T(\gamma)$ being unvanishing. Let $x(z)$ be a sectionally analytic function, i.e., over the domains S_+ and S_- let $x(z)$ equal, respectively, the analytic functions $x_+(z)$ and $x_-(z)$. Then the Cauchy integral

$$x(z) = \frac{1}{2\pi i} \int_\Gamma \frac{F(\zeta)\, d\zeta}{\zeta - z}, \quad (45)$$

solves the problem: find a piecewise analytic function $x(z)$ vanishing at infinity that satisfies on Γ the prescribed transition condition

$$x_+(\gamma) - x_-(\gamma) = F(\gamma), \qquad \gamma \in \Gamma. \quad (46)$$

It must be noted that the function defined as a Cauchy principal value in (45) satisfies a Hölder condition of the same type as F and the Plemelj-Sokhotskii conditions:

$$x_+(\gamma) = x(\gamma) + \frac{1}{2} F(\gamma), \quad (47a)$$

$$x_-(\gamma) = x(\gamma) - \frac{1}{2} F(\gamma). \quad (47b)$$

Moreover, the additional condition $x_-(\infty) = 0$ can be modified. For instance, if $x(z)$ has a pole of order n at $z = \infty$, the solution of (46) is

$$x(z) = \frac{1}{2\pi i} \int_\Gamma \frac{F(\zeta)\, d\zeta}{\zeta - z} + P_n(z), \quad (48)$$

where $P_n(z)$ is a polynomial of order n in z, $P_0(z)$ being a constant.

The Riemann-Hilbert problem is a generalization of this problem. In particular, it is desired to find the sectionally analytic function $x(z)$ which satisfies on the contour Γ either the transition condition

$$x_+(\gamma) = T(\gamma) x_-(\gamma), \quad (49a)$$

or

$$x_+(\gamma) = T(\gamma) x_-(\gamma) + F(\gamma). \quad (49b)$$

A further extension of this problem to open curves and discontinuous coefficients is possible and has been well treated in [8].

Appendix IV

1)

$$R_m = \frac{P_m(\sigma)}{2}, \quad (50)$$

where $P_m(\sigma)$ denotes the Legendre function evaluated at $\sigma = \cos(\psi_0)$ [10].

2)

$$v^r_m = \frac{1}{2\pi} \int_{-\psi_0}^{\psi_0} \frac{e^{-im\psi}}{G_+(e^{i\psi})} \left[\frac{1}{\pi i} \int_\Gamma \frac{G_+(\lambda)\lambda^r}{\lambda - e^{i\psi}} d\lambda\right] d\psi. \quad (51)$$

(a) Referring to [10], we evaluate the following integral

$$\frac{1}{\pi i} \int_\Gamma \frac{G_+(\lambda)\lambda^r}{\lambda - t_0} d\lambda = \frac{1}{2\pi i} \int_G \frac{G_+(\lambda)\lambda^r}{\lambda - t_0} d\lambda,$$

where G is the contour surrounding the arc Γ (Fig. 9). We divide the contour G into two segments C_i and C_0. They are interior and exterior to the unit circle S, respectively. Let us expand the integrand into the following expression [10]:

$$\frac{\sqrt{[(\lambda - e^{i\psi_0})(\lambda - e^{-i\psi_0})]}\lambda^r}{\lambda - t_0} = \begin{cases} -\sum_{j=0}^{\infty} t_0^{-j-1}\lambda^j \sum_{k=0}^{\infty} u_k(\sigma)\lambda^k\lambda^r, & \text{for } |\lambda| < 1 \\ -\sum_{j=0}^{\infty} t_0^j \lambda^{-j} \sum_{k=0}^{\infty} u_k(\sigma)\lambda^{-k}\lambda^r, & \text{for } |\lambda| > 1 \end{cases}$$

where $u_0(\sigma) = 1$, $u_1(\sigma) = -\sigma$, $u_n(\sigma) = P_n(\sigma) - 2\sigma P_{n-1}(\sigma) + P_{n-2}(\sigma)$, $n \geq 2$. The contour integral is evaluated along C_i and C_0 in the clockwise direction. Letting $\epsilon \to 0$ and $R \to \infty$,

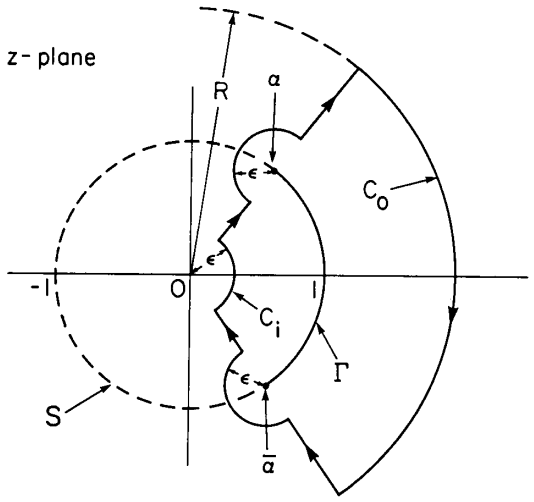

Fig. 9. G is a contour consisting of two segments, C_0 and C_i ($G = C_0 \cup C_i$) which are outside and inside the unit circle S, respectively. Γ is an arc on S, surrounded by the contour G. We define $\Gamma = \{\exp(i\psi) | 0 \le |\psi| \le \psi_0, \psi_0 = c/d\pi\}$, and $\alpha = \exp(i\psi_0)$, $\bar{\alpha} = \exp(-i\psi_0)$. The contour integral in computing v_m^r is carried out along G in the clockwise direction.

we obtain

$$\frac{1}{\pi i}\int_\Gamma \frac{G_+(\lambda)\lambda^r}{\lambda - t_0}\,d\lambda = \frac{\psi_0}{\pi}\left\{\sum_{j=0}^{\infty} t_0^j \sum_{k=0}^{\infty} u_k(\sigma)\ \mathrm{sinc}\ [\psi_0(r-j-k+1)] - \sum_{j=0}^{\infty} t_0^{-j-1}\sum_{k=0}^{\infty} u_k(\sigma)\ \mathrm{sinc}\ [\psi_0(r+j+k+1)]\right\}. \quad (52)$$

We then employ the following equality whose derivation will be given in Appendix IV-b

$$\sum_{n=0}^{\infty} u_n(\sigma)\ \mathrm{sinc}\ [\psi_0(n-r)] = \left(\frac{\pi}{2\psi_0}\right)\sin(\psi_0) P_{r-1}^{-1}(\sigma), \quad (53)$$

where the associated Legendre's function of the first kind is defined by [12, p. 267, eq. (128),]

$$P_n^{-m}(\cos\psi_0) = \frac{2^{-m+1}\sin^{-m}\psi_0}{\Gamma(1/2)\Gamma(m+1/2)} \cdot \int_0^{\psi_0} \frac{\cos(n+1/2)\phi\ d\phi}{(2\cos\phi - 2\cos\psi_0)^{1/2-m}}. \quad (54)$$

Equation (52) can now be simplified to

$$\frac{1}{\pi i}\int_\Gamma \frac{G_+(\lambda)\lambda^r}{\lambda - t_0}\,d\lambda = \frac{1}{2}\left\{\sum_{j=0}^{\infty} t_0^j\,[\sin\psi_0 P_{r-j}^{-1}(\sigma)] - \sum_{j=0}^{\infty} t_0^{-j-1}\,[\sin\psi_0 P_{-r-j-2}^{-1}(\sigma)]\right\}. \quad (55)$$

Substituting (55) into (51) and using the Mehler–Dirichlet formula [10], we have

$$v_m^r = \frac{1}{4}\sum_{j=0}^{\infty}\{P_{j-m-1}(\sigma)P_{r-j}^{-1}(\sigma) - P_{j+m+1}(\sigma)P_{-r-j-2}^{-1}(\sigma)\}\sin\psi_0. \quad (56)$$

With the definition of the function $\sin\psi_0 P_n^{-1}(\sigma)$ given in Appendix IV-b, the following series is derived in a closed form:

$$\begin{aligned}\sum_{j=0}^{\infty} P_{j-m-1}(\sigma)\sin\psi_0 P_{r-j}^{-1}(\sigma) &= \sum_{j=0}^{\infty} P_{m-j}(\sigma)\frac{1}{\pi}\int_{-\psi_0}^{\psi_0}\sqrt{(e^{i\phi}-e^{i\psi_0})(e^{i\phi}-e^{-i\psi_0})}\\ &\quad\cdot\exp[i(r-j)\phi]\,d\phi\\ &= \frac{1}{\pi}\int_{-\psi_0}^{\psi_0}[\mathfrak{F}_m(\phi)\exp(im\phi)\sqrt{e^{i2\phi}-2\sigma e^{i\phi}+1}\\ &\quad\cdot\exp[i(r-m)\phi]\,d\phi \end{aligned} \quad (57)$$

where

$$\mathfrak{F}_m(\phi) = \sum_{j=0}^{\infty} P_{m-j}(\sigma)\exp(-ij\phi).$$

We compute the integration in (57) by parts, where the derivative of the function,

$$\mathfrak{F}_m(\phi)\exp(im\phi)\sqrt{e^{i2\phi}-2\sigma e^{i\phi}+1},$$

with respect to ϕ is derived by taking advantage of the recurrence relationship for $P_n(\sigma)$:

$$(m-j)P_{m-j}(\sigma) - (2m-2j-1)\sigma P_{m-j-1}(\sigma) + (m-j-1)P_{m-j-2}(\sigma) = 0. \quad (58a)$$

In particular, we multiply (58a) by $\exp[i(m-j)\phi]$ and sum over the index j from 0 to ∞. The result can be simplified to

$$\begin{aligned}(1-2\sigma e^{i\phi}+e^{i2\phi})\frac{\partial}{\partial\phi}[\mathfrak{F}_m(\phi)e^{im\phi}] &+ (-i\sigma e^{i\phi}+ie^{i2\phi})[\mathfrak{F}_m(\phi)e^{im\phi}]\\ &= i(m+1)P_m(\sigma)e^{i(m+2)\phi} - i(m+1)P_{m+1}(\sigma)e^{i(m+1)\phi},\end{aligned}$$

Consequently,

$$\frac{\partial}{\partial\phi}\{\mathfrak{F}_m(\phi)e^{im\phi}\sqrt{1-2\sigma e^{i\phi}+e^{i2\phi}}\} = \frac{i(m+1)P_m(\sigma)}{\sqrt{1-2\sigma e^{i\phi}+e^{i2\phi}}} \cdot e^{i(m+2)\phi} - \frac{i(m+1)P_{m+1}(\sigma)}{\sqrt{1-2\sigma e^{i\phi}+e^{i2\phi}}}e^{i(m+1)\phi}. \quad (58b)$$

Using (58b), we can easily compute the integration in (57) by

parts and obtain the following expression for the desired sum:

$$\sum_{j=0}^{\infty} P_{j-m-1}(\sigma)\sin\psi_0 P_{r-j}^{-1}(\sigma)$$

$$= \begin{cases} \left(\dfrac{m+1}{m-r}\right)\{P_m(\sigma)P_{r+1}(\sigma)-P_{m+1}(\sigma)P_r(\sigma)\}, \\ \qquad \text{for } m\neq r,\ m\neq -1 \\ \left(\dfrac{2\psi_0}{\pi}\right)\operatorname{sinc}[\psi_0(r+1)], \qquad \text{for } m\neq r,\ m=-1 \\ (r+1)[P_{r+1}(\sigma)U_r(\sigma)-P_r(\sigma)U_{r+1}(\sigma)], \\ \qquad \text{for } r=m\geq 0 \\ \dfrac{2\psi_0}{\pi}, \qquad \text{for } r=m=-1 \\ (r+1)[P_{-r-1}(\sigma)U_{-r-2}(\sigma)-P_{-r-2}(\sigma)U_{-r-1}(\sigma)], \\ \qquad r=m\leq -2 \end{cases} \tag{59}$$

where

$$U_0(\sigma)=0, \quad U_1(\sigma)=\sigma-1,$$

$$U_{n+1}(\sigma)=\frac{\sigma P_n(\sigma)-P_{n-1}(\sigma)}{(n+1)^2} + \frac{2n+1}{n+1}\sigma U_n(\sigma)-\frac{n}{n+1}U_{n-1}(\sigma), \qquad \text{for } n\geq 1.$$

The case when $r = m$ is given in [6]. The second series in (56) can be derived in a similar fashion. Consequently, the parameter v_m^r expressed by (56) has the closed-form representation:

$$v_m^r = \begin{cases} \dfrac{(m+1)}{2(m-r)}[P_m(\sigma)P_{r+1}(\sigma)-P_{m+1}(\sigma)P_r(\sigma)], \\ \qquad m\neq r \\ \dfrac{m+1}{2}[P_{m+1}(\sigma)U_m(\sigma)-P_m(\sigma)U_{m+1}(\sigma)], \\ \qquad m=r\geq 0 \\ 0, \qquad m=r=-1 \\ \dfrac{m+1}{2}[P_{-m-1}(\sigma)U_{-m-2}(\sigma)-P_{-m-2}(\sigma)U_{-m-1}(\sigma)], \\ \qquad m=r\leq -2. \end{cases}$$

(b) Derivation of (53) in Appendix IV-b: Let us consider the associated Legendre's function $P_{r-1}^{-1}(\cos\psi_0)$ defined in (54), [12]

$$P_{r-1}^{-1}(\cos\psi_0)=P_{-r}^{-1}(\cos\psi_0) = \frac{\sin^{-1}\psi_0}{\pi}\int_{-\psi_0}^{\psi_0}\exp(-ir\phi) \cdot\sqrt{(e^{i\phi}-e^{i\psi_0})(e^{i\phi}-e^{-i\psi_0})}\,d\phi. \tag{60}$$

Since [10]

$$\sum_{n=0}^{\infty} u_n(\sigma)\exp(in\phi) = \begin{cases} \sqrt{(e^{i\phi}-e^{i\psi_0})(e^{i\phi}-e^{-i\psi_0})}, & 0\leq|\phi|<\psi_0 \\ (-)\sqrt{(e^{i\phi}-e^{i\psi_0})(e^{i\phi}-e^{-i\psi_0})}, & \psi_0<|\phi|\leq\pi \end{cases},$$

(60) can be written as

$$\sin(\psi_0)P_{r-1}^{-1}(\sigma)=\frac{1}{\pi}\int_{-\psi_0}^{\psi_0}\exp(-ir\phi)\cdot\sum_{n=0}^{\infty}u_n(\sigma)\exp(in\phi)\,d\phi = \frac{2\psi_0}{\pi}\sum_{n=0}^{\infty}u_n(\sigma)\operatorname{sinc}[\psi_0(n-r)].$$

Equation (53) follows immediately.

3)

$$w^r=\sum_{\substack{m=-\infty\\ m\neq 0}}^{\infty}\frac{v_m^r(-1)^m}{m}.$$

Substituting (56) for v_m^r into the above equation, we have

$$w^r=\frac{1}{4}\sum_{j=0}^{\infty}\sin\psi_0 P_{r-j}^{-1}(\sigma)\left[\sum_{m\neq 0}\frac{(-1)^m P_{m-j}(\sigma)}{m}\right] -\frac{1}{4}\sum_{j=0}^{\infty}\sin\psi_0 P_{-r-j-2}^{-1}(\sigma)\left[\sum_{m\neq 0}\frac{(-1)^m P_{j+m+1}(\sigma)}{m}\right]. \tag{61}$$

With (59) and the following equality [10, eq. (38)]:

$$\sum_{m=-\infty}^{\infty}\frac{(-1)^m P_{m-k}(\sigma)}{m+s}=\frac{\pi}{\sin(s\pi)}P_{s+k-1}(\sigma),$$

the series in (61) can be evaluated in the limit as $s \to 0$. This yields

$$w^r = \begin{cases} -\dfrac{1}{2}\sin\psi_0 P_r^{-1}(\sigma)\ln\left(\dfrac{1+\sigma}{2}\right) \\ \quad +\dfrac{1}{2r}[P_r(\sigma)-P_{r-1}(\sigma)], \qquad r\neq 0. \\ \dfrac{(1+\sigma)}{2}\ln\left(\dfrac{1+\sigma}{2}\right), \qquad r=0. \end{cases}$$

4)

$$Y=\sum_{\substack{m=-\infty\\ m\neq 0}}^{\infty}\frac{R_m(-1)^m}{m}=-\frac{1}{2}\ln\left(\frac{1+\sigma}{2}\right).$$

See [10] for this derivation.

REFERENCES

[1] R. Kastner and Mittra, "A spectral-iteration technique for analyzing a corrugated-surface twist polarizer for scanning reflector antennas," *IEEE Trans. Antennas Propagat.*, vol. AP-30, pp. 673–676, July 1982.

[2] R. Petit, *Electromagnetic Theory of Gratings, Topics in Current Physics*. New York: Springer-Verlag, 1980.

[3] T. K. Gaylord and M. G. Moharam, "Analysis and applications of optical diffraction gratings," *Proc. IEEE*, vol. 73, no. 5, pp. 894–938, May 1985.

[4] J. A. DeSanto, "Scattering from a perfectly reflecting arbitrary periodic surface: An exact theory," *Radio Sci.*, vol. 16, no. 6, pp. 1315–1326, Nov.-Dec. 1981.

[5] Y. L. Kok and N. C. Gallagher, "Relative phases of electromagnetic waves diffracted by a perfectly conducting rectangular-groove grating," *J. Opt. Soc. Am. A*, vol. 5, pp. 65–73, Jan. 1988.

[6] W. A. Johnson and R. W. Ziolkowski, "The scattering of an *H*-polarized plane wave from an axially slotted infinite cylinder: A dual series approach," *Radio Sci.*, vol. 19, no. 1, pp. 275–291, Jan.-Feb. 1984.

[7] R. W. Ziolkowski, W. A. Johnson, and K. F. Casey, "Application of Riemann–Hilbert problem techniques to electromagnetic coupling through apertures," *Radio Sci.*, vol. 19, no. 6, pp. 1425–1431, Nov.-Dec. 1984.

[8] R. W. Ziolkowski, "*n*-series problems and the coupling of electromagnetic waves to apertures: A Riemann–Hilbert approach," *SIAM J. Math. Ann.*, vol. 16, no. 2, pp. 358–378, Mar. 1985.

[9] R. W. Ziolkowski and J. B. Grant, "Scattering from cavity-backed apertures: The generalized dual series solution of the concentrically loaded *E*-pol slit cylinder problem," *IEEE Trans. Antennas Propagat.*, vol. AP-35, no. 5, pp. 504–528, May 1987.

[10] Z. S. Agronovich, V. A. Marchenko, and V. P. Shestopalov, "The diffraction of electromagnetic waves from plane metallic lattices," *Soviet Phys.-Tech. Phys.*, vol. 7, no. 4, pp. 277–286, Oct. 1962.

[11] F. D. Gakhov, *Boundary Value Problems*. Elmsford, NY: Pergamon, 1966.

[12] E. W. Hobson, *Spherical and Ellipsoidal Harmonics*. New York: Chelsea, 1955.

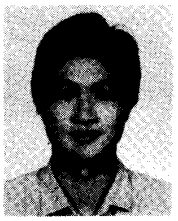

Yon-Lin Kok (S'83–M'83–S'84–M'86–S'87–A'88) was born in Tainan, Taiwan, Republic of China, in 1958. He received the B.S. degree in electrophysics from National Chiao-Tung University, Tsin-Chu, Taiwan, in 1980, the M.S. degree in electrical engineering from Michigan State University, East Lansing, in 1983, and the Ph.D. degree from Purdue University, West Lafayette, IN, in 1988.

He was a Research Assistant at Michigan State University studying image synthesis and restoration within a diffraction-limited optical system. He is now an Assistant Professor in the Department of Electrical Engineering, University of South Alabama, Mobile, AL. His research interests include electromagnetic scattering from rough surfaces, diffraction gratings, optics and image processing.

Neal C. Gallagher, Jr. (S'72–M'75–SM'85–F'87) received the Ph.D. degree in electrical engineering in 1974 from Princeton University, Princeton, NJ.

He was with the Faculty of Case Western Reserve University, Cleveland, OH, and joined Purdue University, West Lafayette, IN, in 1976, where he is currently a Professor of Electrical Engineering. He is the President of Gallagher Associates, Inc., doing research and system design in microwave holography, diffractive optics, guidance systems, and signal processing.

Richard W. Ziolkowski (M'87) for a photograph and biography please see page 528 of the May 1987 issue of this TRANSACTIONS.